

Evolution of the phenomenologically determined collective potential along the chain of Zr isotopesE. V. Mardyban,^{1,2} E. A. Kolganova^{1,2}, T. M. Shneidman^{1,3} and R. V. Jolos^{1,2}¹*Joint Institute for Nuclear Research, 141980 Dubna, Moscow Region, Russia*²*Dubna State University, 141982 Dubna, Moscow Region, Russia*³*Kazan Federal University, Kazan 420008, Russia*

(Received 25 November 2021; accepted 4 February 2022; published 22 February 2022)

Background: The properties of the collective low-lying states of Zr isotopes which include excitation energies and $E2$ reduced transition probabilities indicate that some of these states are mainly spherical and the other are mainly deformed ones. A consideration of these data in the framework of the geometrical collective model with β , γ , and rotational degrees of freedom is necessary for $^{92-102}\text{Zr}$.

Purpose: To investigate the properties of the low-lying collective states of $^{92-102}\text{Zr}$ based on the five-dimensional geometrical quadrupole collective model, to obtain the collective potentials for the chain of Zr isotopes and to investigate their evolution with increase of the number of neutrons.

Method: The quadrupole-collective Bohr Hamiltonian depending on both β and γ shape variables with a potential having spherical and deformed minima is applied. The relative depth of two minima, height and width of the barrier, and rigidity of the potential near both minima are determined so as to achieve the best possible description of the observed properties of the low-lying collective quadrupole states of $^{92-102}\text{Zr}$.

Results: Satisfactory agreement with the experimental data on the excitation energies and the $E2$ reduced transition probabilities is obtained. The evolution of the collective potential with increase of A is described and the distributions of the wave functions of the collective states in β - γ plane are found.

Conclusion: It is shown that the low-energy structure of $^{92-102}\text{Zr}$ can be described in a satisfactory way within the geometrical collective model with the Bohr Hamiltonian. The β dependence of the potential energy is fixed to describe the experimental data in a best possible way. The resulting potential evolves with A increase from having only one spherical minimum in ^{92}Zr , through the potentials having both spherical and deformed minima, to the potential with one deformed minimum in ^{102}Zr . A β dependence of the wave functions is presented in a set of figures illustrating their distribution over β .

DOI: [10.1103/PhysRevC.105.024321](https://doi.org/10.1103/PhysRevC.105.024321)**I. INTRODUCTION**

Zr isotopes are of particular interest for investigation of nuclear structure, especially because they are characterized by a dramatic transition from spherical to deformed shape at low excitation energies [1,2]. Many spectroscopic data have been accumulated for these nuclei [3–18] containing information on excitation energies and electromagnetic transition probabilities. Various theoretical approaches have been used to study shape phase transitions in these nuclei [2,19–60]. Theoretical studies of Zr isotopes can be divided into two groups. The first group was aimed to clarify the mechanism of a sharp transition from the spherical shape to the deformed one. These investigations were based either on the nuclear shell model [19–32], or on the self-consistent mean field, the Strutinsky-type approaches to calculations of the potential energy surface [33–40], and the energy density functional [41–44]. The interacting boson model based on the mean field calculations was also used to describe the properties of Zr isotopes [45–47]. The second group includes studies based mainly on the phenomenological models: the interacting boson model or the interacting boson model with configuration mixing

[48–54], or on the Bohr collective Hamiltonian [56–58]. In Refs. [59,60], two-level mixing model has been used to analyze experimental data.

In this work, the consideration of the low-lying states of $^{92-102}\text{Zr}$ is based on the five-dimensional Bohr Hamiltonian. The aim of this work is to determine the collective potentials for the $^{92-102}\text{Zr}$ isotopes fixing their β dependence so as to obtain the better possible description of the experimental data and investigate the evolution of the collective potential with increase of the number of neutrons. The other aim is to get a distribution of the wave functions of the low-lying collective states in β - γ plane.

This consideration is not free from restrictions. A certain dependence of the potential on a variable describing nonaxial deformation is assumed and restrictions on the inertia tensor are imposed.

II. HAMILTONIAN

In the general case, the quadrupole collective Bohr Hamiltonian can be presented as (see Ref. [56])

$$H = -\frac{\hbar^2}{2\sqrt{\omega r}} \left(\frac{1}{\beta^4} \left[\frac{\partial}{\partial \beta} \sqrt{\frac{r}{\omega}} \beta^4 B_{\gamma\gamma} \frac{\partial}{\partial \beta} - \frac{\partial}{\partial \beta} \sqrt{\frac{r}{\omega}} \beta^3 B_{\beta\gamma} \frac{\partial}{\partial \gamma} \right] \right. \\ \left. + \frac{1}{\beta \sin 3\gamma} \left[-\frac{\partial}{\partial \gamma} \sqrt{\frac{r}{\omega}} \sin 3\gamma B_{\beta\gamma} \frac{\partial}{\partial \beta} + \frac{1}{\beta} \frac{\partial}{\partial \gamma} \sqrt{\frac{r}{\omega}} \sin 3\gamma B_{\beta\beta} \frac{\partial}{\partial \gamma} \right] \right) + \frac{1}{2} \sum_{k=1}^3 \frac{\hat{J}_k^2}{\mathfrak{S}_k(\beta)} + V(\beta, \gamma). \quad (1)$$

Here $\omega = B_{\beta\beta} B_{\gamma\gamma} - B_{\beta\gamma}^2$ is the determinant of the vibrational part of the inertia tensor

$$B_{vib} = \begin{pmatrix} B_{\beta\beta} & \beta B_{\beta\gamma} \\ \beta B_{\beta\gamma} & \beta^2 B_{\gamma\gamma} \end{pmatrix}, \quad (2)$$

and $r = B_1 B_2 B_3$, where B_k ($k = 1, 2, 3$) are presented in the expression for the components of the moment of inertia \mathfrak{S}_k determined with respect to the body-fixed axes as

$$\mathfrak{S}_k = 4B_k(\beta) \beta^2 \sin^2 \left(\gamma - \frac{2\pi k}{3} \right). \quad (3)$$

The components of the angular momentum in the body-fixed frame are denoted as \hat{J}_k and can be expressed in terms of the Euler angles. The potential energy is denoted as $V(\beta, \gamma)$. The Hamiltonian (1) is a general case of the conventional Bohr Hamiltonian [61], allowing the nonzero value of $B_{\beta\gamma}$.

To simplify consideration, we make below the following assumptions for the inertia coefficients:

$$B_{\beta\beta} = B_{\gamma\gamma} = B_0, \quad B_{\beta\gamma} = 0, \\ B_1(\beta) = B_2(\beta) = B_3(\beta) = b_{rot}(\beta) B_0, \quad (4)$$

where B_0 is the parameter scaling vibrational and rotational inertia coefficients. With respect to the value of b_{rot} , it is known [62,63] that in the deformed nuclei b_{rot} is less than one. In the region of a small values of β we put $b_{rot} = 1$ (see discussion in Ref. [58]). Since a general feature of the collective potential used below is the presence of two minima, spherical and deformed, separated by the barrier at $\beta = \beta_m$, we set b_{rot} as follows:

$$b_{rot} = \begin{cases} 1 & \text{if } \beta \leq \beta_m, \\ b_{def} < 1 & \text{if } \beta > \beta_m. \end{cases} \quad (5)$$

The change from the spherical to deformed value of b_{rot} occurs at $\beta = \beta_m$, which is taken around the maximum of the barrier separating spherical and deformed potential wells. Our calculations show that the small variations of β_m do not affect qualitatively the results of the calculations.

With these assumptions about inertia tensor, the Hamiltonian (1) takes the form

$$\hat{H} = -\frac{\hbar^2}{2B_0} \left(\frac{1}{b_{rot}^{3/2}} \frac{1}{\beta^4} \frac{\partial}{\partial \beta} \beta^4 b_{rot}^{3/2} \frac{\partial}{\partial \beta} + \frac{1}{\beta^2 \sin 3\gamma} \frac{\partial}{\partial \gamma} \sin 3\gamma \frac{\partial}{\partial \gamma} \right) \\ + \frac{1}{2} \sum_{k=1}^3 \frac{\hat{J}_k^2}{\mathfrak{S}_k(\beta)} + V(\beta, \gamma). \quad (6)$$

We expect that the wave functions of the lowest states are localized in the minima while the weight of the wave functions inside the barrier region is strongly suppressed. In this case,

we can neglect a derivative of b_{rot} over β which is presented, in principle, in the kinetic part of the Hamiltonian (6), as it gives the nonzero contribution to the matrix elements of the Hamiltonian only in the barrier region where the wave functions are close to zero. Thus, we obtain finally the following model Hamiltonian:

$$H = -\frac{\hbar^2}{2B_0} \left(\frac{1}{\beta^4} \frac{\partial}{\partial \beta} \beta^4 \frac{\partial}{\partial \beta} + \frac{1}{\beta^2 \sin 3\gamma} \frac{\partial}{\partial \gamma} \sin 3\gamma \frac{\partial}{\partial \gamma} \right) \\ + \sum_{k=1}^3 \frac{\hat{J}_k^2}{4b_{rot} \beta^2 \sin \left(\gamma - \frac{2\pi k}{3} \right)} + V(\beta, \gamma), \quad (7)$$

The aim of the present work is to determine the potential energy in the Bohr Hamiltonian for nuclei belonging to the chain of the Zr isotopes so as to achieve the best possible agreement with the experimental data in excitation energies and $E2$ transition probabilities for the low-lying states. This give us the possibility to explore the evolution of the collective potential with increase of A along the chain of Zr isotopes. The potential energy $V(\beta, \gamma)$ in (7) is chosen in the form

$$V(\beta, \gamma) = U(\beta) + C_\gamma \beta^3 (1 - \cos 3\gamma). \quad (8)$$

Thus, we fix the dependence of V on γ , eliminating potentials with minimum corresponding to the nonaxial shapes. The form of $U(\beta)$ and the parameter C_γ , which determines the stiffness of the potential with respect to γ oscillations at the deformed minimum, are fitted to reproduce the experiment data.

In our previous work [57], to describe the shape of $U(\beta)$ for ^{96}Zr we have defined several points fixing the positions of the spherical and deformed minima, the rigidity of the potential near its minima, and the height and width of the barrier separating two minima. Then we vary the positions of the selected points in order to get a satisfactory description of the experimental data. The number of points was taken to be 16 to provide a smooth change of the potential with β . However, we have found that not all the points are of the same physical importance and that the number of points can be minimized as, obviously, the only relative depths of the minima and the height and width of the barrier leads to physically meaningful changes.

For this reason, in the present paper we approximate the potential by the three parabolas: two to describe spherical and deformed minima, and the inverted parabola to describe the barrier separating two minima. The potential was constructed by smooth cross-linking of the three parabolas. The bottom of the parabola corresponding to spherical minimum was fixed at $\beta_2 = 0$ and at zero energy. The adjusted parameters are as

TABLE I. Parameters of the potential and the rotational inertia coefficient. w_{sph} (w_{def}) is the stiffness of the parabola describing the spherical (deformed) minimum; β_{def} is the location of the deformed minimum at β axis; h_{def} is the height of the location of the bottom of the parabola describing deformed minimum with respect to the bottom of the spherical minimum; h_b is the height of the top of the parabola describing the barrier.

Isotope	w_{sph} (MeV)	w_{def} (MeV)	β_{def}	h_{def} (MeV)	h_b (MeV)	b_{def}
^{92}Zr	933.8	296.6	0.34	4.5	4.5	0.37
^{94}Zr	235.4	200	0.35	2.7	3.2	0.25
^{96}Zr	958	453.4	0.25	5.2	6.7	0.23
^{98}Zr	843.4	200	0.23	4.4	5.5	0.29
^{100}Zr	1027.6	200	0.33	1.1	2	0.27
^{102}Zr	899.2	326.4	0.29	-3.8	0	0.42

follows: stiffness of the parabola describing spherical minimum (w_{sph}); stiffness of the parabola describing deformed minimum (w_{def}); location at β_2 axis (β_{def}) and the height with respect to the bottom of the spherical minimum (h_{def}) of the parabola describing deformed minimum; and the height of the top of the parabola defining the barrier (h_b). The obtained parameters for the Zr isotopes are shown in Table I together with value of the rotational inertia coefficient in deformed region.

To solve the eigenvalue problem with the Hamiltonian (7), we expand the eigenfunctions in terms of a complete set of basis functions that depends on the deformation variables β and γ and the Euler angles. These functions are well known and their construction is described in the literature. See, for instance, Refs. [64,65] and references below. For completeness of presentation, we give some details here.

For each value of angular momentum I , the basis functions are written as

$$\Psi_{IM}^{n_\beta v \alpha} = R^{(n_\beta, v)}(\beta) \Upsilon_{v\alpha IM}(\gamma, \Omega), \quad (9)$$

where $\Upsilon_{v\alpha IM}$ are the $\text{SO}(5) \supset \text{SO}(3)$ spherical harmonics, which are the eigenfunctions of the operator $\hat{\Lambda}^2$:

$$\begin{aligned} \hat{\Lambda}^2 \Upsilon_{v\alpha IM} &= \left[-\frac{1}{\sin 3\gamma} \frac{\partial}{\partial \gamma} \sin 3\gamma \frac{\partial}{\partial \gamma} + \frac{1}{4} \sum_k \frac{\hat{f}_k^2}{\sin^2(\gamma - \frac{2\pi k}{3})} \right] \Upsilon_{v\alpha IM} \\ &= v(v+3) \Upsilon_{v\alpha IM}. \end{aligned} \quad (10)$$

In addition to the angular momentum I and its projection M , each function $\Upsilon_{v\alpha IM}$ is labeled by the $\text{SO}(5)$ seniority quantum number v and a multiplicity index α , which is required for $v \geq 6$.

The $\Upsilon_{v\alpha IM}$ can be explicitly constructed as a sum over the functions with explicit value of the projection K of the angular momentum on the intrinsic axis [66,67]

$$\Upsilon_{v\alpha IM}(\gamma, \Omega) = \sum_{K=0, \text{even}}^I F_{v\alpha I, K}(\gamma) \xi_{KM}^I(\Omega), \quad (11)$$

where

$$\xi_{KM}^I(\Omega) = \frac{1}{\sqrt{2(1+\delta_{K0})}} [D_{MK}^I(\Omega) + (-1)^I D_{M-K}^I(\Omega)] \quad (12)$$

and the $F_{v\alpha I, K}(\gamma)$ are polynomials constructed from the trigonometrical functions of γ [68]. This construction is used in the present work.

The basis wave functions $R^{(n_\beta, v)}$ are chosen as the eigenfunctions of the harmonic oscillator Hamiltonian in β :

$$h_{h.o.} = \frac{1}{2} \left(-\frac{1}{\beta^4} \frac{\partial}{\partial \beta} \beta^4 \frac{\partial}{\partial \beta} + \frac{v(v+3)}{\beta^2} + \frac{\beta^2}{\beta_0^4} \right). \quad (13)$$

The eigenfunctions of $h_{h.o.}$ have the following analytical form,

$$R_{n_\beta, v}(\beta) = N_\beta \left(\frac{\beta}{\beta_0} \right)^v L_{n_\beta}^{v+3/2} \left(\frac{\beta^2}{\beta_0^2} \right) \exp \left(-\frac{\beta^2}{2\beta_0^2} \right), \quad (14)$$

where β_0 is an oscillator length and the normalization constant N_β is given as

$$N_\beta = \sqrt{\frac{2n_\beta!}{\Gamma(n_\beta + v + 5/2)}}. \quad (15)$$

The basis functions $R_{n_\beta, v}$ are completely specified by the choice of the oscillator length β_0 . Our calculations have shown that the fastest convergence of the results is obtained when β_0 is chosen to be equal to the value at the region of the barrier separating two minima, so that the oscillator potential coincides with the potential $U(\beta)$ at the top of the barrier. For such a choice of β_0 , $(n_\beta)_{\text{max}} = 30$ is enough to provide a convergence. The basis of harmonics $\Upsilon_{v\alpha IM}(\gamma, \Omega)$ is truncated to some maximum seniority v_{max} . As shown in Ref. [69], taking $v_{\text{max}} = 50$ is sufficient to provide a convergence of the calculation.

The Hamiltonian eigenfunctions Ψ_{InM} , where n is a multiplicity index, are obtained in calculations as a series expansions in the basic functions (9). For discussions below it is convenient to introduce the one-dimensional probability distribution over β determined by integration of $|\Psi_{InM}|^2$ over γ and Euler angles:

$$\beta^4 \int_0^{\pi/3} \sin 3\gamma d\gamma \int d\Omega |\Psi_{InM}|^2. \quad (16)$$

The collective quadrupole operator responsible for $E2$ transitions is taken in the form

$$\begin{aligned} Q_{2\mu} &= \frac{3Ze}{4\pi} R_0^2 \left(\beta \cos \gamma D_{\mu 0}^2(\Omega) \right. \\ &\quad \left. + \frac{1}{\sqrt{2}} \beta \sin \gamma (D_{\mu 2}^2(\Omega) + D_{\mu -2}^2(\Omega)) \right). \end{aligned} \quad (17)$$

III. RESULTS

The results of calculations of the excitation energies and the $E2$ reduced transition probabilities are presented in Tables II and III.

TABLE II. Comparison of the experimental and calculated energies of the low-lying collective states of the even-even $^{92-102}\text{Zr}$ isotopes. The observed 2_2^+ state in ^{92}Zr has a noncollective nature and is presented for the completeness only. For this reason, the calculated excitation energy of this state is not shown in this table. Experimental data are taken from Ref. [71].

A	92		94		96		98		100		102	
	Exp	Calc										
$E(0_2^+)$	1.38	1.35	1.30	1.30	1.58	1.58	0.85	0.86	0.33	0.33	0.90	0.90
$E(0_3^+)$	2.90	2.10		1.57	2.70	2.40	1.44	1.63	0.83	0.80		1.38
$E(2_1^+)$	0.93	0.91	0.92	0.95	1.75	1.75	1.22	1.18	0.21	0.19	0.15	0.15
$E(2_2^+)$	1.85	–	1.67	1.61	2.23	2.00	1.59	1.59	0.83	0.88	1.04	1.02
$E(2_3^+)$	2.07	1.77	2.15	1.92	2.67	2.79	1.75	2.00	1.20	1.22	1.21	1.21
$E(3_1^+)$	2.91	2.91	2.51	3.19	2.44	3.74		2.80	1.40	1.75	1.24	1.32
$E(4_1^+)$	1.50	1.88	1.47	1.98	2.86	2.69	1.84	1.86	0.56	0.56	0.48	0.47
$E(4_2^+)$	2.40	2.56	2.33	2.07	3.08	3.34	2.05	2.53	1.41	1.43	1.39	1.39
$E(4_3^+)$	2.87	2.90	2.86	2.77	3.18	3.68	2.28	2.95	1.86	1.89	1.54	1.68

A. ^{92}Zr

Let us take a closer look at the results of calculations for ^{92}Zr . In this nucleus, the value of the $B(E2; 2_1^+ \rightarrow 0_1^+)$ of 6.4 W.u. indicates the collective nature of the 2_1^+ state related to the oscillations of the nuclear shape around the spherical one. Of course, ^{92}Zr is not the right nucleus to consider in a collective model. It has only two valence nucleons, and even taking into account a possible transition of the pair of protons from $p_{1/2}$ to $g_{9/2}$ single-particle levels,

this increases the number of valence nucleons to six only. Nevertheless, we include this nucleus into consideration, since our main task is to obtain the most complete information on the evolution of the collective potential along the Zr isotope chain. In Tables II and III, the experimental data and the results of our calculations for the low-lying states of ^{92}Zr are compared. The calculated value of the $B(E2; 2_1^+ \rightarrow 0_1^+) = 8.2$ W.u. is close to the experimental value 6.4 W.u. Comparison of the experimental $E2$ reduced transition probabilities from 2_2^+ (1847 keV) and 2_3^+ (2067 keV) states to 2_1^+ state

TABLE III. Comparison of the experimental and calculated $E2$ reduced transition probabilities between the low-lying states of the even-even $^{92-102}\text{Zr}$ isotopes. The observed 2_2^+ state has a noncollective nature and is presented for the completeness only. For this reason, the calculated values of the $E2$ reduced transition probabilities from and to this state are not shown in the table. Experimental data are taken mainly from Ref. [71].

A	92		94		96		98		100		102	
	Exp	Calc	Exp	Calc	Exp	Calc	Exp	Calc	Exp	Calc	Exp	Calc
$B(E2; 0_2 \rightarrow 2_1)$	14.4(5)	20.74	9.4(4)	12.94	4.90				67(6)	26.35		10.37
$B(E2; 2_1 \rightarrow 0_2)$							$29\binom{+8}{-6}$	29.02				
$B(E2; 2_1 \rightarrow 0_1)$	6.4(6)	8.17	4.9(3)	8.09	$2.3(3)^b$	3.69	$2.9\binom{+8}{-5}$	1.84	77(2)	64.70	105(14)	53.94
$B(E2; 2_2 \rightarrow 0_1)$	3.7(5)		$3.9(3)^a$	0.00	$0.26(8)^c$	0.26		2.58		0.00		1.40
$B(E2; 2_2 \rightarrow 0_2)$			$19(2)^a$	31.59	$36(11)^c$	33.84		3.00		18.10		23.55
$B(E2; 2_2 \rightarrow 2_1)$	$0.001\binom{+25}{-1}$		$0.06\binom{+0.13}{-0.06}^c$	1.52	$2.8\binom{+1.5}{-1.0}^d$	3.86		12.56		3.49		9.79
$B(E2; 2_3 \rightarrow 0_1)$	<0.0042	0.02		0.01		0.01		0.25		0.53		1.92
$B(E2; 2_3 \rightarrow 2_1)$	<15	16.27		13.76	$50(7)^b$	3.07		9.90		0.03		0.03
$B(E2; 3_1 \rightarrow 2_1)$	0.030(7)	0.04		0.03	$0.1\binom{+0.3}{-0.1}^b$	0.15		1.93		4.49		5.00
$B(E2; 3_1 \rightarrow 2_2)$	2.4(14)			3.59		3.14		3.79		0.08		42.70
$B(E2; 4_1 \rightarrow 2_1)$	4.05(12)	17.65	0.879(23)	4.19	$16\binom{+5}{-13}^b$	6.86	$42\binom{+10}{-7}$	46.99	101.4(11)	104.41	$167\binom{+30}{-22}^e$	81.49
$B(E2; 4_1 \rightarrow 2_2)$				88.07	$56(44)^b$	55.76	$54\binom{+18}{-16}$	11.29		12.76		0.31
$B(E2; 4_2 \rightarrow 2_1)$	5.9(7)	0.002	$13\binom{+4}{-7}^a$	12.08		7.04		1.00		0.03		0.15
$B(E2; 4_2 \rightarrow 2_2)$			$34\binom{+10}{-17}^a$	15.22		2.29		17.41		58.67		50.37
$B(E2; 4_2 \rightarrow 4_1)$	2.3(13)	5.55		12.26		3.30		9.87		3.73		9.43
$B(E2; 4_3 \rightarrow 2_1)$	0.76(15)	0.01		0.04		0.21		0.02		0.58		0.73
$B(E2; 4_3 \rightarrow 4_1)$	2.7(6)	6.84		1.16		6.16		1.92		2.71		0.32
$B(E2; 4_3 \rightarrow 4_2)$	$0.03\binom{+99}{-3}$	8.93		4.56		0.13		8.97		11.48		6.64

^aExperimental data are taken from Ref. [12].

^bExperimental data are taken from Ref. [72].

^cExperimental data are taken from Ref. [14].

^dExperimental data are taken from Ref. [17].

^eExperimental data are taken from Ref. [15].

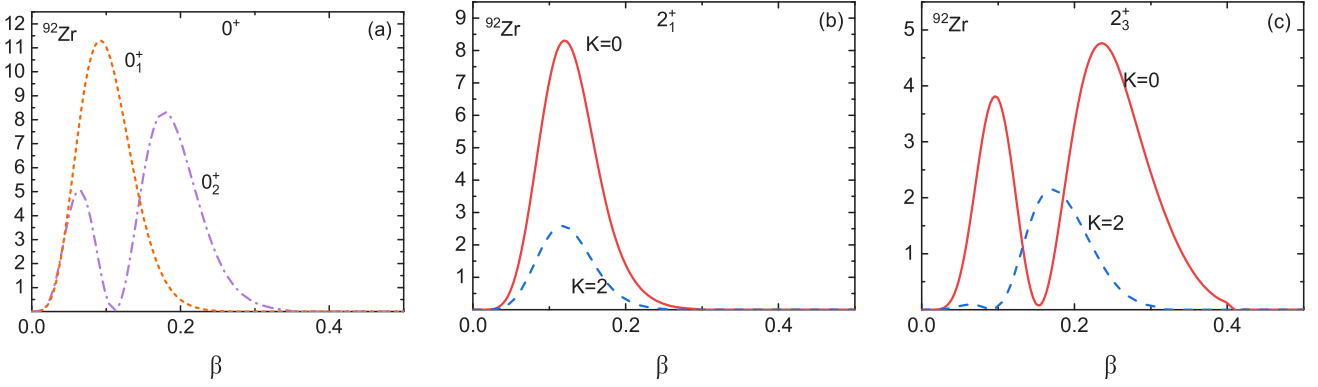


FIG. 1. Distribution over β of the squares of the wave functions or their components in ^{92}Zr determined by Eq. (16). (a) 0_1^+ (red short dashed line) and 0_2^+ (purple dash-dotted line) states. (b) 2_1^+ state ($K=0$, red solid line; $K=2$, blue dashed line). (c) 2_3^+ state ($K=0$, red solid line; $K=2$, blue dashed line).

with the calculated ones shows that the calculated state with excitation energy 1770 keV is close in properties to the experimentally observed 2_3^+ (2067 keV) state. That is why in the tables the calculated state with the excitation energy of 1770 keV is compared with the observed 2_3^+ state. Thus, we have the $B(E2; 2_3^+ \rightarrow 2_1^+)_{\text{exp}} \leq 15$ W.u. and the $B(E2; 2_3^+ \rightarrow 2_1^+)_{\text{cal}} = 16.3$ W.u. Further, the $B(E2; 2_3^+ \rightarrow 0_1^+)_{\text{exp}} < 0.004$ W.u. and the $B(E2; 2_3^+ \rightarrow 0_1^+)_{\text{cal}} = 0.02$ W.u. This comparison indicates the collective nature of the 2_3^+ state, which is confirmed by the small value of the $B(M1; 2_3^+ \rightarrow 2_1^+)$. A small value of the $B(E2; 2_2^+ \rightarrow 2_1^+)_{\text{exp}} = 0.001$ W.u. and a large value of the $B(M1; 2_2^+ \rightarrow 2_1^+)_{\text{exp}}$ indicates on the noncollective nature of the experimentally observed 2_2^+ state. Therefore, description of the observed 2_2^+ state requires the shell model consideration and is not considered in this paper. For this reason, the results of calculations of the $E2$ reduced transition probabilities from the 2_2^+ state and to this state are not given in Table III.

The experimental value of the $B(E2; 0_2^+ \rightarrow 2_1^+)_{\text{exp}} = 14.4$ W.u. indicates the collective nature of the 0_2^+ state. From this point of view, it is in a correspondence with the calculated value of the $B(E2; 0_2^+ \rightarrow 2_1^+)_{\text{cal}} = 20.7$, although the calculated value is significantly larger than the experimental one. Comparison of the experimental and calculated values of the $B(E2; 4_1^+ \rightarrow 2_1^+)$, 4.05 and 17.7 W.u., correspondingly, indicates on the presence in the wave function of the 4_1^+ state of the shell model configuration $(d_{5/2}d_{5/2})_4$. This explains the strong discrepancy between the experimental and calculated results. The proximity in the value of the experimental $E2$ reduced transition probabilities $B(E2; 4_1^+ \rightarrow 2_1^+)_{\text{exp}}$ and $B(E2; 4_2^+ \rightarrow 2_1^+)_{\text{exp}}$ indicates that the lowest energy pure collective 4^+ state generated by the Bohr collective Hamiltonian is fragmented, and distributed between the experimentally observed 4_1^+ and 4_2^+ states. This statement is consistent with the fact that the calculated value of $B(E2; 4_2^+ \rightarrow 2_1^+)$ is practically zero.

In Fig. 1, a β dependence of the wave functions of the 2_1^+ , 0_2^+ , and 2_3^+ states of ^{92}Zr is demonstrated. It is seen that the wave functions of the 0_2^+ and 2_3^+ states have a similar β dependence; namely, they have a node in β in contrast to the 2_1^+ state. This makes these states similar to the

two-phonon states, which explains the large value of the $E2$ reduced transition probability from these states to the 2_1^+ state. Our calculations qualitatively confirm these experimental data.

B. ^{94}Zr

Let us consider the experimental data on ^{94}Zr . The experimental value of $B(E2; 2_1^+ \rightarrow 0_1^+) = 4.9$ W.u. indicates that the 2_1^+ state of this nucleus is quite collective, and its structure is formed by excitation of both proton and neutron subsystems. However, the predominance of the neutron shell model configuration $(d_{5/2}d_{5/2})_2$, whose contribution to the value of the $B(E2; 2_1^+ \rightarrow 0_1^+)$ is small, cannot be excluded. This possibility is indicated by the value of $B(E2; 2_1^+ \rightarrow 0_1^+)_{\text{cal}} = 8.09$ W.u. calculated using the standard definition of the quadrupole moment operator in the geometrical collective model. Comparing this value with the experimental one, it can be assumed that the contribution of a noncollective component to the wave function of the 2_1^+ state may be of the order of 50%.

The experimental value of $B(E2; 4_1^+ \rightarrow 2_1^+)_{\text{exp}}$ is noticeably less than $B(E2; 2_1^+ \rightarrow 0_1^+)_{\text{exp}}$, which indicates on a predominance of the noncollective component $(d_{5/2}d_{5/2})_4$ in the structure of the 4_1^+ state, either on a deformed nature of the 4_1^+ state in contrast to the spherical 2_1^+ state. Our calculations support a second possibility. At the same time, a large experimental value of the $B(E2; 4_2^+ \rightarrow 2_1^+)_{\text{exp}} = 13.2$ W.u. indicates that 4_2^+ state is the spherical one as the 2_1^+ state. This interpretation is confirmed by the β dependence of the wave function of the 4_2^+ state [see Fig. 2(e)] which is concentrated at low β , as the wave function of the 2_1^+ state and has a node in β . The wave function of the 4_1^+ state is concentrated at large β [see Fig. 2(d)]. This explains the small value of the $B(E2; 4_1^+ \rightarrow 2_1^+)$. Our calculations of the $B(E2; 4_1^+ \rightarrow 2_1^+)$ confirm the experimentally observed tendency to decrease $B(E2; 4_1^+ \rightarrow 2_1^+)$ compared to $B(E2; 2_1^+ \rightarrow 0_1^+)$, although it gives a value exceeding the experimental one.

Interpretation of the properties of the 2_2^+ state is complicated. The large experimental value of $B(E2; 4_2^+ \rightarrow 2_2^+)$ qualitatively reproduced by our calculations (however, twice

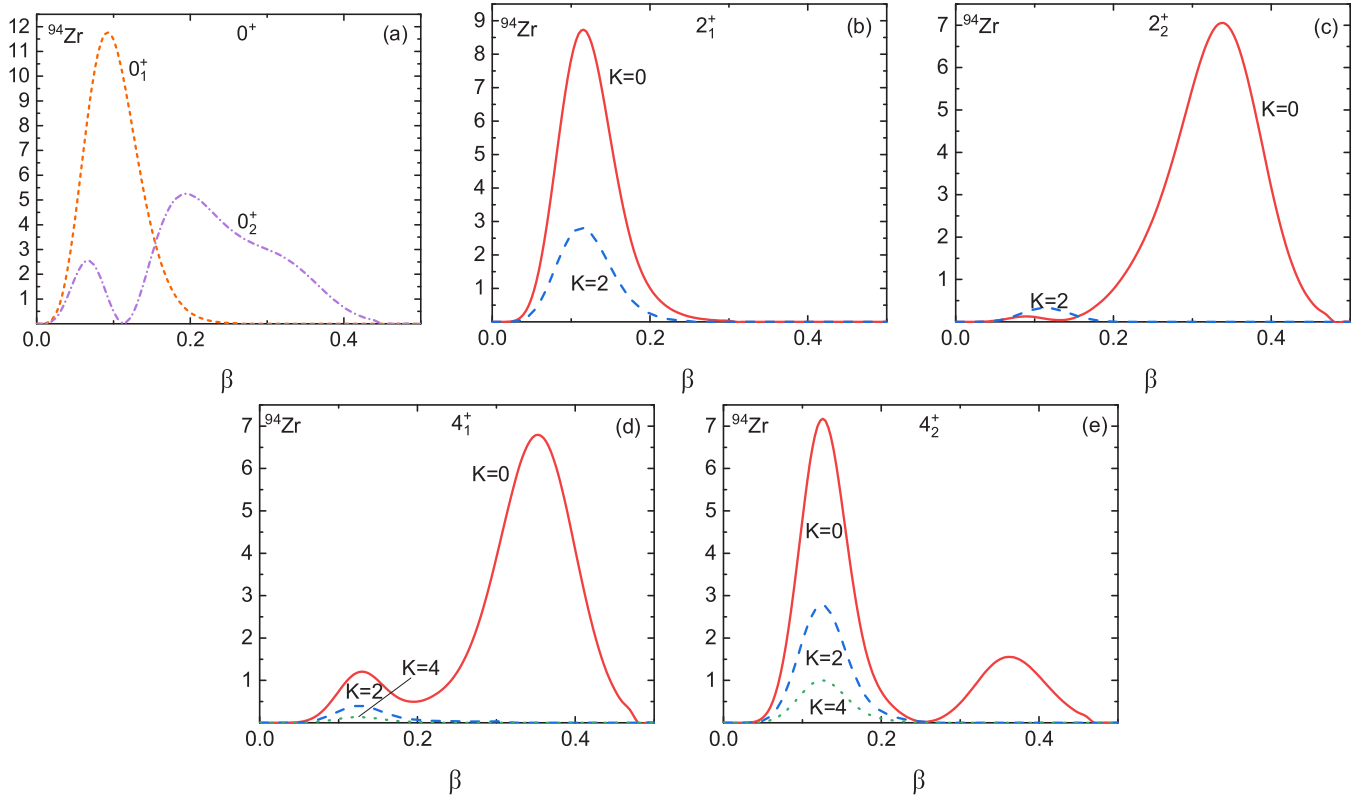


FIG. 2. Distribution over β of the squares of the wave functions or their components in ^{94}Zr determined by Eq. (16). (a) 0_1^+ (red short dashed line) and 0_2^+ (purple dash-dotted line) states. (b) 2_1^+ state ($K=0$, red solid line; $K=2$, blue dashed line). (c) 2_2^+ state ($K=0$, red solid line; $K=2$, blue dashed line). (d) 4_1^+ state ($K=0$, red solid line; $K=2$, blue dashed line; $K=4$, blue). (e) 4_2^+ state ($K=0$, red solid line; $K=2$, blue dashed line; $K=4$, green dotted line).

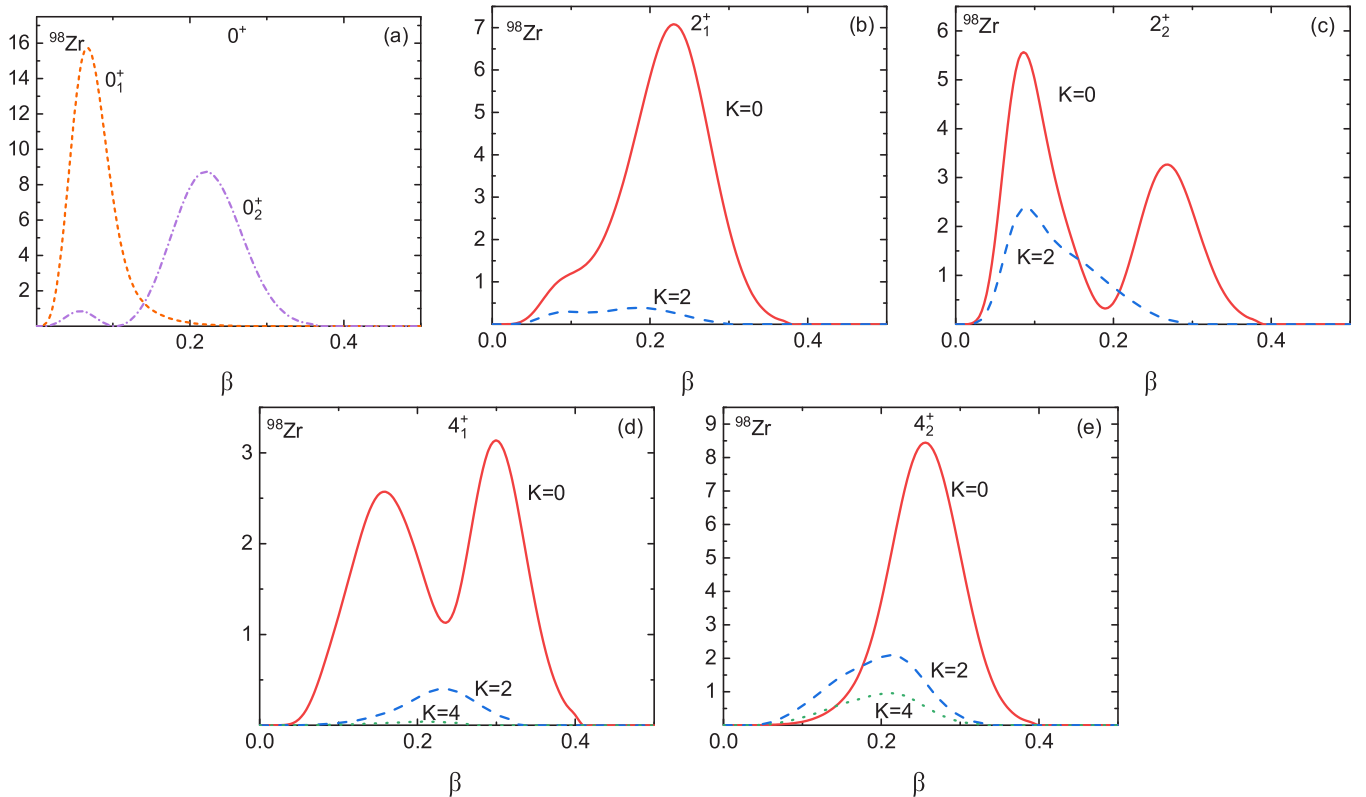


FIG. 3. The same as in Fig. 2, but for ^{98}Zr .

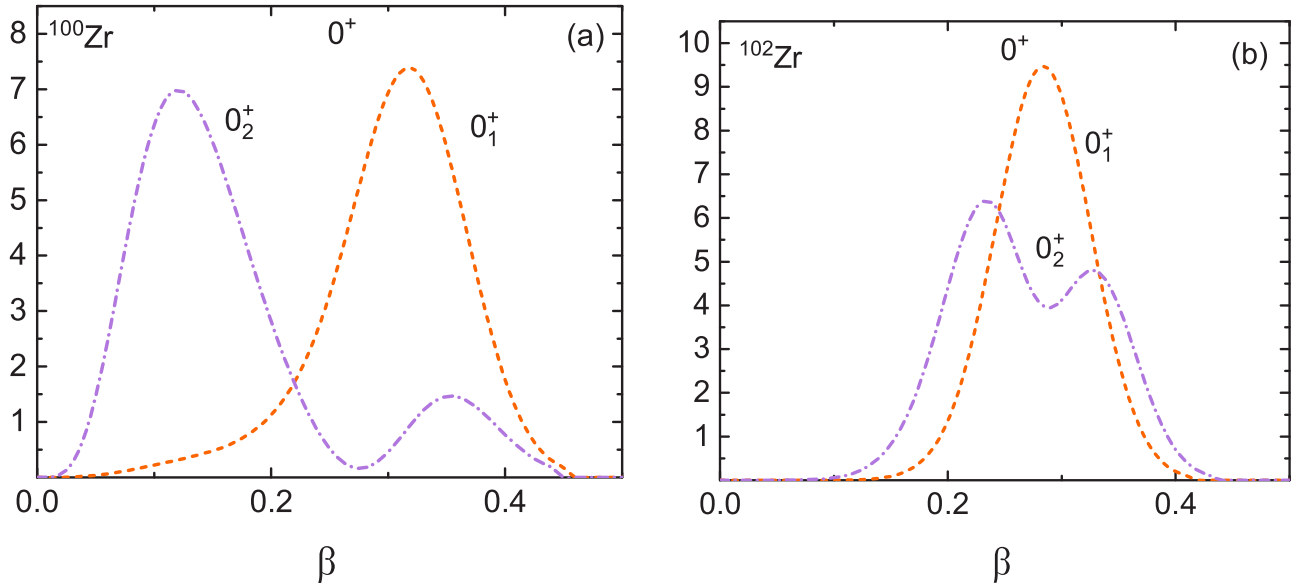


FIG. 4. Distribution over β of the squares of the wave functions of the 0_1^+ (red short-dashed line) and 0_2^+ (purple dash-dotted line) states determined by Eq. (16). (a) ^{100}Zr . (b) ^{102}Zr .

as less) assumes a spherical nature of the 2_2^+ state in agreement with a spherical nature of the 4_2^+ state. At the same time, a small experimental value of the $B(E2; 2_2^+ \rightarrow 2_1^+)$ contradicts the assumption of the spherical structure of the 2_2^+ state, because the 2_1^+ state is spherical as seen in Fig. 2(b). As shown in Fig. 2(c), the 2_2^+ state is deformed and the relatively large value of $B(E2; 4_2^+ \rightarrow 2_2^+)$ is explained by the presence of the second maximum of the wave function of the 4_2^+ state at large values of β . Deformed structure of the 2_2^+ state explains a small value of the $B(E2; 2_2^+ \rightarrow 2_1^+)$. The calculated value of $B(E2; 2_2^+ \rightarrow 0_1^+)$ is small, in agreement with a deformed structure of the 2_2^+ state and spherical nature of the 0_1^+ state. However, the fact that the calculated value of the $B(E2; 2_2^+ \rightarrow 0_1^+)$ is significantly less than the experimental value indicates that the calculated 2_2^+ state too much shifted into deformed region.

A large value of $B(E2; 0_2^+ \rightarrow 2_1^+)$ indicates that 0_2^+ state can be similar in its structure to the two-phonon state, although modified by the anharmonic effects. At the same time, a large value of the $B(E2; 2_2^+ \rightarrow 0_2^+)$, which is also reproduced by our calculations, is rather consistent with the deformed structure of the 0_2^+ state. In Fig. 2(a), the square of the wave function of the 0_2^+ state is presented as a function of β . It is seen that from one side the wave function of the 0_2^+ state has a node as a function of β , which makes the 0_2^+ state similar to the two-phonon state. This explains a large value of the $B(E2; 0_2^+ \rightarrow 2_1^+)$. But from the other side, a large part of the wave function of the 0_2^+ state is located in the region of large β . It explains the large value of the $B(E2; 2_2^+ \rightarrow 0_2^+)$.

C. ^{96}Zr

The nucleus ^{96}Zr was considered in details in our previous publication [58], albeit with slightly different parametrization of the potential energy. The results shown in Tables II and III are close to those shown in Ref. [58]. Some of the values calculated in this work are closer to the experimental values

than those obtained in Ref. [58]. In several cases, previous results are better agreed with experimental data. This applies to $B(E2; 4_1^+ \rightarrow 2_1^+)$ and $B(E2; 4_2^+ \rightarrow 2_2^+)$.

D. ^{98}Zr

The wave functions of the low-lying states of ^{98}Zr are shown in Fig. 3. It is seen that the wave function of the 0_1^+ state is concentrated around $\beta \approx 0.1$, i.e., in the spherical region, but the 0_2^+ state is deformed.

The wave function of the 2_1^+ state has a wide maximum centered at $\beta = 0.27$, i.e., is distributed over both spherical and deformed regions. A similar structure has a wave function of the 4_2^+ state. The wave functions of the 2_2^+ and 4_1^+ states are similar to each other. The squares of their wave functions has two maxima: one spherical and the other deformed.

The following $E2$ transitions are measured: $B(E2; 0_2^+ \rightarrow 2_1^+)_{\text{exp}} = 29.0$ W.u. and $B(E2; 2_1^+ \rightarrow 0_1^+)_{\text{exp}} = 2.9$ W.u. The large value of the $B(E2; 0_2^+ \rightarrow 2_1^+)_{\text{exp}}$ is explained by the fact that the wave functions of both 0_2^+ and 2_1^+ states have a similar structure and are located in deformed region. The relatively small value of the $B(E2; 2_1^+ \rightarrow 0_1^+)_{\text{exp}}$ is explained by the fact that the wave function of the 0_1^+ state is concentrated in a spherical region, in contrast to the 0_2^+ state.

A large experimental value of the $B(E2; 4_1^+ \rightarrow 2_1^+)_{\text{exp}} = 42$ W.u. is reproduced in calculations: $B(E2; 4_1^+ \rightarrow 2_1^+)_{\text{cal}} = 47$ W.u. It is explained by the fact that the wave function of the 2_1^+ state is located in deformed region, and the wave function of the 4_1^+ has a strong maximum in the same region. The calculated value of the $B(E2; 4_1^+ \rightarrow 2_2^+)_{\text{cal}} = 11.3$ W.u. is characteristic for the collective $E2$ transition. However, its value is five times smaller than the experimental one. Probably, this means that the maximum of the wave function of the 2_2^+ state located at $\beta = 0.1$ should be lower than that obtained in our calculations and shown in Fig. 3(c). However, deformed maximum of this wave function should be higher than that shown in Fig. 3(c).

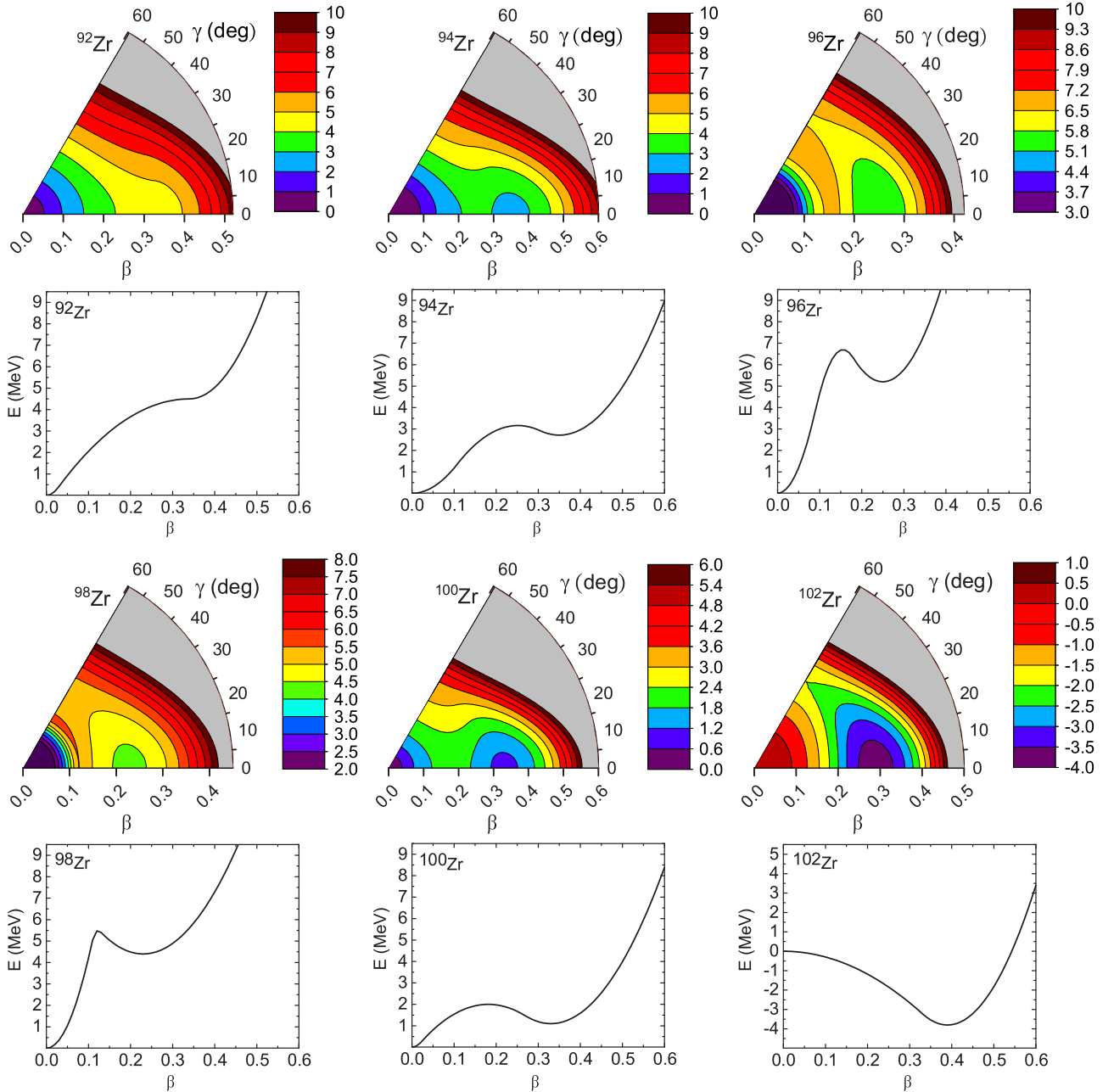


FIG. 5. Collective potential for the even-even Zr isotopes obtained by fitting the experimental data for the low-lying collective quadrupole states.

E. $^{100,102}\text{Zr}$

In ^{100}Zr we consider only two quasirotational bands based on 0_1^+ and 0_2^+ states. The more strong $E2$ transitions connect the states of the ground band based on the 0_1^+ . The results of calculations of these transitions are in agreement with the experimental data. Unfortunately, there are no experimental data for $E2$ transitions between the states of the second band. The calculated values of $B(E2)$ for this band are noticeably smaller than those for transitions within the ground band. However, they are strong enough to confirm their collective nature. Calculated values of the $E2$ transitions between rotational bands are small compared to probabilities of the $E2$ transitions

inside rotational bands. Based on the values of $B(E2)$ for transitions inside the bands, we conclude that the rotational band based on 0_1^+ state is rather deformed and that based on the 0_2^+ is more spherical. This conclusion is supported by the calculated β dependence of the wave functions of the 0_1^+ and 0_2^+ states shown in Fig. 4(a).

The experimental data and the results of calculation for ^{102}Zr present a picture similar to that described above for ^{100}Zr . In ^{102}Zr there is a rotational band based on the ground state, with strong $E2$ transitions between the states of the band. This indicates that the 0_1^+ state is deformed. The excited band is based on the 0_2^+ state with the calculated excitation

energy 900 keV. This band is characterized by fairly collective, but still weaker than in the case of the ground band, $E2$ transitions within the band. The calculated excitation energy of the 0_2^+ state indicates that excited band can be interpreted as a quasi- β band. However, smaller calculated values of the $E2$ transition probabilities inside this band indicate that the 0_2^+ wave function has an admixture of the spherical component. Wave functions of the 0_1^+ and 0_2^+ states are shown in Fig. 4(b). From Fig. 4(b), it is seen that the wave function of the 0_2^+ state oscillates like the wave function of the β -vibrational state. However, it is shifted to the spherical region with a greater extent than the wave function of the 0_1^+ state.

F. Potential

The resulting potentials $V(\beta, \gamma)$ for all considered Zr isotopes are presented in Fig. 5, where the value of C_γ is taken to be positive. Our calculations have shown that the results are not very sensitive to the exact value of the parameter C_γ . For ^{96}Zr its value was fixed as $C_\gamma = 50$ MeV to provide better fit of the experimental data [58]. No significant changes were found in the calculated results for the excitation energies and the $E2$ transition probabilities when C_γ was varied around 50 MeV. Therefore, to reduce the number of adjustable parameters, we fix the same value of C_γ for all considered Zr isotopes.

The β dependence of the collective potential taken for $\gamma = 0$ is illustrated in Fig. 5. It is seen that in $^{94,96,98,100}\text{Zr}$ spherical and deformed minima coexist. In ^{92}Zr the deformed minimum is only intended. In ^{94}Zr deformed minimum is very shallow, in $^{96,98,100}\text{Zr}$ it is clearly isolated, and in ^{102}Zr there is only deformed minimum.

It is seen in Fig. 5 that the spherical minimum of the potential in $^{96,98}\text{Zr}$ is more rigid than in lighter Zr isotopes. This fact correlates with the higher energies of the 2_1^+ states in $^{96,98}\text{Zr}$ compare to $^{92,94}\text{Zr}$. This result is in accordance

with the single-particle level scheme of Zr isotopes given in Ref. [70]. According to this scheme, the lowest neutron single-particle level in the shell above $N = 50$ is $d_{5/2}$. The following single-particle level $s_{1/2}$ is located above $d_{5/2}$ by 1033 keV, and the single-particle level $g_{7/2}$ is separated from $s_{1/2}$ by 1940 keV. Thus, single-particle neutron states $d_{5/2}$ and $s_{1/2}$ play the role of subshells and this explains a larger rigidity of the potential near the spherical minimum in $^{96,98}\text{Zr}$, in contrast to the lighter Zr isotopes.

IV. CONCLUSION

We have studied a possibility to describe the properties of the low-lying collective quadrupole states of $^{92-102}\text{Zr}$ based on the five-dimensional Bohr collective Hamiltonian. Both β and γ shape collective variables are included into consideration. The β dependence of the potential energy is fixed to describe the experimental data in a best possible way. However, the γ dependence of the potential is introduced in a simple way favoring axial symmetry at large β . The resulting potential evolve with A increase from having only one spherical minimum, through the potentials having both spherical and deformed minima, to the potential with one deformed minimum in ^{102}Zr .

A detailed comparison of the energy spectra, the $E2$ transition probabilities, and a discussion of the characteristics of the resulting wave functions was carried out. A β dependence of the wave functions is presented in a set of figures illustrating their distribution over β at $\gamma = 0$.

ACKNOWLEDGMENTS

The authors express their gratitude to the RFBR (Grant No. 20–02–00176) and to the Heisenberg–Landau Program for support. One of the authors, T.M.S., acknowledges support from Russian Government Subsidy Program of the Competitive Growth of Kazan Federal University.

-
- [1] K. Heyde and J. L. Wood, *Rev. Mod. Phys.* **83**, 1467 (2011).
 [2] J. E. García-Ramos and K. Heyde, *Phys. Rev. C* **100**, 044315 (2019).
 [3] K. Kawade, G. Battistuzzi, H. Lawin, H. A. Seli, K. Sistemich, F. Schussler, E. Monnard, J. A. Pinston, B. Pfeiffer, and G. Jung, *Z. Phys. A* **304**, 293 (1982).
 [4] J. Ebert and K. Sistemich (eds.), *Nuclear Structure of the Zirconium Region, Proceedings of the International Workshop* (Springer-Verlag, Berlin, 1988).
 [5] H. Mach, M. Moszynski, R. Gill, F. Wahn, J. Winger, J. C. Hill, G. Molnar, and K. Sistemich, *Phys. Lett. B* **230**, 21 (1989).
 [6] H. Mach, F. K. Wahn, G. Molnar, K. Sistemich, John C. Hill, M. Moszynski, R. L. Gill, W. Krips, and D. S. Brenner, *Nucl. Phys. A* **523**, 197 (1991).
 [7] G. Lhersonneau, B. Pfeiffer, K.-L. Kratz, T. Enqvist, P. P. Jauho, A. Jokinen, J. Kantele, M. Leino, J. M. Parmonen, H. Penttilä, and J. Äystö (ISOLDE Collaboration), *Phys. Rev. C* **49**, 1379 (1994).
 [8] W. Urban, T. Rzaca-Urban, J. L. Druell, W. R. Phillips, A. G. Smith, B. J. Varley, I. Ahmad and N. Schulz, *Nucl. Phys. A* **689**, 605 (2001).
 [9] C. Y. Wu, H. Hua, D. Cline, A. B. Hayes, R. Teng, R. M. Clark, P. Fallon, A. Goergen, A. O. Macchiavelli, and K. Vetter, *Phys. Rev. C* **70**, 064312 (2004).
 [10] U. Hager, T. Eronen, J. Hakala, A. Jokinen, V. S. Kolhinen, S. Kopecky, I. Moore, A. Nieminen, M. Oinonen, S. Rinta-Antila, J. Szerypo, and J. Äystö, *Phys. Rev. Lett.* **96**, 042504 (2006).
 [11] C. Goodina, Y. X. Luoab, J. K. Hwanga, A. V. Ramayya, J. H. Hamiltona, J. O. Rasmussen, S. J. Zhuc, A. Gelberg, and G. M. Ter-Akopian, *Nucl. Phys. A* **787**, 231 (2007).
 [12] A. Chakraborty, E. E. Peters, B. P. Crider, C. Andreoiu, P. C. Bender, D. S. Cross, G. A. Demand, A. B. Garnsworthy, P. E. Garrett, G. Hackman, B. Hadinia, S. Ketelhut, Ajay Kumar, K. G. Leach, M. T. McEllistrem, J. Pore, F. M. Prados-Estevéz, E. T. Rand, B. Singh, E. R. Tardiff *et al.*, *Phys. Rev. Lett.* **110**, 022504 (2013).
 [13] F. Browne, A. M. Bruce, T. Sumikama, I. Nishizuka, S. Nishimura, P. Doornenbal, G. Lorusso, P.-A. Söderström, H. Watanabe, R. Daido, Z. Patel, S. Rice, L. Sinclair, J. Wu, Z. Y. Xu, A. Yagi, H. Baba, N. Chiga, R. Carroll, F. Didierjean, Y. Fang *et al.*, *Phys. Lett. B* **750**, 448 (2015).

- [14] C. Kremer, S. Aslanidou, S. Bassauer, M. Hilcker, A. Krugmann, P. von Neumann-Cosel, T. Otsuka, N. Pietralla, V. Y. Ponomarev, N. Shimizu, M. Singer, G. Steinhilber, T. Togashi, Y. Tsunoda, V. Werner, and M. Zweidinger, *Phys. Rev. Lett.* **117**, 172503 (2016).
- [15] S. Ansari, J. M. Regis, J. Jolie, N. Saed-Samii, N. Warr, W. Korten, M. Zielinska, M.-D. Salsac, A. Blanc, M. Jentschel, U. Köster, P. Mutti, T. Soldner, G. S. Simpson, F. Drouet, A. Vancraeynest, G. de France, E. Clement, O. Stezowski, C. A. Ur *et al.*, *Phys. Rev. C* **96**, 054323 (2017).
- [16] P. Singh, W. Korten, T. W. Hagen, A. Görge, L. Grente, M.-D. Salsac, F. Farget, E. Clement, G. de France, T. Braunroth, B. Bruyneel, I. Celikovic, O. Delaune, A. Dewald, A. Dijon, J.-P. Delaroche, M. Girod, M. Hackstein, B. Jacquot, J. Libert *et al.*, *Phys. Rev. Lett.* **121**, 192501 (2018).
- [17] W. Witt, N. Pietralla, V. Werner, and T. Beck, *Eur. Phys. J. A* **55**, 79 (2019).
- [18] V. Werner, W. Witt, T. Beck, N. Pietralla, M. Boromiza, C. Clisu, C. Costache, I. E. Dinescu, A. Ionescu, P. R. John, P. Koseoglou, N. Marginen, R. Marginen, C. Mihai, R. E. Mihai, A. Mitu, A. Negret, C. R. Nita, A. Olacel, S. Pascu, A. Serban, C. Sotty *et al.*, *Eur. Phys. J. WEB Conf.* **223**, 01070 (2019).
- [19] P. Federman and S. Pittel, *Phys. Lett. B* **77**, 29 (1978).
- [20] P. Federman and S. Pittel, *Phys. Rev. C* **20**, 820 (1979).
- [21] A. Kumar and M. R. Gunye, *Phys. Rev. C* **32**, 2116 (1985).
- [22] A. Holt, T. Engeland, M. Hjorth-Jensen, and E. Osnes, *Phys. Rev. C* **61**, 064318 (2000).
- [23] F. R. Xu, P. M. Walker, and R. Wyss, *Phys. Rev. C* **65**, 021303(R) (2002).
- [24] K. Sieja, F. Nowacki, K. Langanke, and G. Martinez-Pinedo, *Phys. Rev. C* **79**, 064310 (2009).
- [25] T. Togashi, Yu. Tsunoda, T. Otsuka, and N. Shimizu, *Phys. Rev. Lett.* **117**, 172502 (2016).
- [26] P.-G. Reinhard, D. J. Dean, W. Nazarewicz, J. Dobaczewski, J. A. Maruhn, and M. R. Strayer, *Phys. Rev. C* **60**, 014316 (1999).
- [27] A. Petrovici, *Phys. Rev. C* **85**, 034337 (2012).
- [28] M. Sugita and A. Arima, *Nucl. Phys. A* **515**, 77 (1990).
- [29] C. Özen and D. J. Dean, *Phys. Rev. C* **73**, 014302 (2006).
- [30] S. Verma, P. A. Dar, and R. Devi, *Phys. Rev. C* **77**, 024308 (2008).
- [31] Y.-X. Liu, Y. Sun, X.-H. Zhou, Y.-H. Zhang, S.-Y. Yu, Y.-C. Yang, and H. Jin, *Nucl. Phys. A* **858**, 11 (2011).
- [32] E. T. Gregor, M. Scheck, M. Chapman, L. P. Gaffney, J. Keatings, K. R. Mashtakov, D. O'Donnell, J. F. Smith, P. Spagnoletti, M. Thurauf, V. Werner, and C. Wiseman, *Eur. Phys. J. A* **53**, 50 (2017).
- [33] S. Miyahara and H. Nakada, *Phys. Rev. C* **98**, 064318 (2018).
- [34] P. Bonche, H. Flocard, P. H. Hennen, S. J. Krieger, and M. S. Weiss, *Nucl. Phys. A* **443**, 39 (1985).
- [35] D. Galeriu, D. Bucurescu, and M. Ivascu, *J. Phys. G* **12**, 329 (1986).
- [36] P. Möler, J. R. Nix, W. D. Myers, and W. J. Swiatecki, *At. Data Nucl. Data Tables* **59**, 185 (1995).
- [37] J. Skalski, S. Mizutori, and W. Nazarewicz, *Nucl. Phys.* **617**, 282 (1997).
- [38] J. Skalski, P.-H. Heenen, and P. Bonche, *Nucl. Phys. A* **559**, 221 (1993).
- [39] R. Rodríguez-Guzmán, P. Sarriguren, L. M. Robledo, and S. Perez-Martin, *Phys. Lett. B* **691**, 202 (2010).
- [40] J.-P. Delaroche, M. Girod, J. Libert, H. Goutte, S. Hilaire, S. Peru, N. Pillet, and G. F. Bertsch, *Phys. Rev. C* **81**, 014303 (2010).
- [41] G. A. Lalazissis, S. Raman, and P. Ring, *At. Data Nucl. Data Tables* **71**, 1 (1999).
- [42] J. Xiang, Z. P. Li, Z. X. Li, J. M. Yao, and J. Meng, *Nucl. Phys. A* **873**, 1 (2012).
- [43] H. Mei, J. Xiang, J. M. Yao, Z. P. Li, and J. Meng, *Phys. Rev. C* **85**, 034321 (2012).
- [44] T. Nikšić, D. Vretenar, and P. Ring, *Prog. Part. Nucl. Phys.* **66**, 519 (2011).
- [45] K. Nomura, R. Rodríguez-Guzmán, and L. M. Robledo, *Phys. Rev. C* **94**, 044314 (2016).
- [46] T. Otsuka and Y. Tsunoda, *J. Phys. G* **43**, 024009 (2016).
- [47] A. Vitturi, in *Nuclear Theory*, edited by M. Gaidarov and N. Minkov (Heron Press, Sofia, 2017), Vol. 37.
- [48] S. Lalkovski and P. Van Isacker, *Phys. Rev. C* **79**, 044307 (2009).
- [49] P. Van Isacker, A. Bouldjedri, and S. Zerguine, *Nucl. Phys. A* **836**, 225 (2010).
- [50] M. Böyükata, P. Van Isacker, and I. Uluer, *J. Phys. G* **37**, 105102 (2010).
- [51] J. E. García-Ramos, K. Heyde, R. Fossion, V. Hellemans, and S. De Baerdemacker, *Eur. Phys. J. A* **26**, 221 (2005).
- [52] N. Gavrielov, A. Leviatan, and F. Iachello, *Phys. Rev. C* **99**, 064324 (2019).
- [53] N. Gavrielov, A. Leviatan, and F. Iachello, *Phys. Scr.* **95**, 024001 (2020).
- [54] J. E. Garcia-Ramos and K. Heyde, *Phys. Rev. C* **102**, 054333 (2020).
- [55] J. R. Stone, P. A. M. Guichon, P. G. Reinhard, and A. W. Thomas, *Phys. Rev. Lett.* **116**, 092501 (2016).
- [56] T. Nikšić, Z. P. Li, D. Vretenar, L. Prochniak, J. Meng, and P. Ring, *Phys. Rev. C* **79**, 034303 (2009).
- [57] D. A. Sazonov, E. A. Kolganova, T. M. Shneidman, R. V. Jolos, N. Pietralla, and W. Witt, *Phys. Rev. C* **99**, 031304(R) (2019).
- [58] E. V. Mardyban, E. A. Kolganova, T. M. Shneidman, R. V. Jolos, and N. Pietralla, *Phys. Rev. C* **102**, 034308 (2020).
- [59] H. T. Fortune, *Phys. Rev. C* **95**, 054313 (2017).
- [60] H. T. Fortune, *Phys. Rev. C* **100**, 034303 (2019).
- [61] A. Bohr, *Dan. Mat.-Fys. Medd.* **26**, 1 (1952).
- [62] R. V. Jolos and P. von Brentano, *Phys. Rev. C* **76**, 024309 (2007).
- [63] R. V. Jolos and P. von Brentano, *Phys. Rev. C* **77**, 064317 (2008).
- [64] D. R. Bes, *Nucl. Phys.* **10**, 373 (1959).
- [65] G. G. Dussel and D. Bes, *Nucl. Phys. A* **143**, 623 (1970).
- [66] D. J. Rowe, P. S. Turner, and J. Repka, *J. Math. Phys.* **45**, 2761 (2004).
- [67] M. A. Caprio, D. J. Rowe, and T. A. Welsh, *Comput. Phys. Commun.* **180**, 1150 (2009).
- [68] D. J. Rowe and J. L. Wood, *Fundamentals of Nuclear Models: Foundational Models* (World Scientific, Singapore, 2010).
- [69] M. A. Caprio, *Phys. Rev. C* **83**, 064309 (2011).
- [70] A. H. Taqi and Z. Q. Mosa, *Egypt. J. Phys.* **48**, 1 (2020).
- [71] <http://www.nndc.bnl.gov/ensdf/>.
- [72] D. Abriola and A. A. Sonzogni, *Nucl. Data Sheets* **109**, 2501 (2008).